# Determination of the scattering potential for low energy alkali-metal ions from a Mo(001) surface

S. H. Overbury and D. R. Huntley
*Oak Ridge National Laboratory, Oak Ridge, Tennessee 37831*
(Received 15 July 1985)

The scattering potential for $Li^+$, $Na^+$, and $K^+$ ions reflected from Mo(001) has been determined for incident energies of 250, 500, and 2500 eV. This was done by measuring the dependence of scattered intensity as a function of incident polar angle for various total scattering angles for each ion and incident energy. The angle of the sharp cutoff in intensity is compared with the critical angle predicted by the chain model. It is found that at 2500 eV the scattering is adequately described by the Thomas-Fermi-Moliere potential with use of a Firsov screening length reduced by factors of 0.90, 0.95, and 1.0 for $Li^+$, $Na^+$, and $K^+$, respectively. The data are also described by a universal potential proposed by Ziegler, Biersack, and Littmark. Systematic disagreement between computed and experimental cutoff angles exists at low incident energy and low scattering angle. This can be attributed either to a breakdown of the chain approximation or to an additional repulsive term in the scattering potential which is dependent upon the distance from the surface.

## I. INTRODUCTION

An important problem in applying low energy ion scattering to the analysis of solid surfaces is to obtain scattering potentials which accurately describe the interaction between the probe ions and the surface atoms. A realistic form of the scattering potential must be known in order to calculate shadow cone or single scattering cross sections and for computer simulations of scattered energy and angle distributions from three-dimensional crystal surfaces. Such computations are necessary to obtain surface composition, surface structure, or adsorbate bonding geometry from measured ion scattering data.

The scattering potentials which are most generally used to describe ion scattering at low and medium energies ($\gtrsim$500 eV) are universal pairwise potentials based on a screened Coulomb potential:

$$V(r)=\frac{Z_1Z_2e^2}{r}\phi(r/a)\ , \tag{1}$$

where $Z_1$ and $Z_2$ are the atomic numbers of projectile and target, respectively, and $r$ is their separation. Various forms of the screening function $\phi$ and of the screening length $a$ have been proposed. Perhaps the most common form is the Moliere approximation to the Thomas-Fermi[1] screening function, which takes the form

$$\phi(x)=0.35\exp(-0.3x)+0.55\exp(-1.2x)+0.10\exp(-6.0x)\ . \tag{2a}$$

Various forms for the screening length have been proposed, and a common form is the value suggested by Firsov,[2]

$$a=Ca_F=C(0.8853)a_B(Z_1^{1/2}+Z_2^{1/2})^{-2/3}\ , \tag{2b}$$

where $a_B$ is the Bohr radius, 0.529 Å. The adjustable parameter $C$ does not appear in the theory of Firsov, but has been proposed by numerous researchers to improve agreement with experimental results. Therefore, the Thomas-Fermi-Moliere (TFM) potential, described by Eqs. (1) and (2), has one adjustable parameter. Recently, Ziegler, Biersack, and Littmark[3] (ZBL) have proposed another empirical form of the screening function which was formulated by fitting a four-term sum of exponential screening function to the potentials computed from Hartree-Fock calculations for many different projectile target combinations. This universal function has the form

$$\phi_{\rm ZBL}=0.1818\exp(-3.2x)+0.5099\exp(-0.9423x)+0.2802\exp(-0.4029x)+0.02817\exp(-0.2016x)\ , \tag{3a}$$

$$a=0.8853a_B(Z_1^{0.23}+Z_2^{0.23})^{-1}\ , \tag{3b}$$

and contains no adjustable parameters. Recent work by Hulpke and Mann[4] has revealed that for low energies (6–36 eV) the scattering cannot be described by only a pairwise interaction such as Eq. (1) depending only upon $r$. They found it necessary to include a potential term which depends upon the distance from the surface $z$, including an attractive term due to the image charge and a repulsive term which becomes important for regions of the surface between atoms.

One method of obtaining a scattering potential from low energy ion scattering is to measure the dependence of the ion scattering intensity upon the polar angle of incidence $\psi$ measured from the plane of the surface. This is done in a particular azimuth aligned with rows of surface atoms where the spacing between atoms of the row is known. The method is based on the assumption that the scattering is approximated by scattering from surface chains of atoms. No scattering can occur into a given laboratory scattering angle $\theta$ for incidence below the critical angle $\psi_c$, because each atom of the chain is in the shadow

 

cone of the preceding atom. This results in an abrupt edge or cutoff in intensity as $\psi$ is decreased below $\psi_c$. If the chain approximation is valid, the critical angle $\psi_c$ depends upon the scattering angle in a way which can be readily calculated for various scattering potentials. Comparison of the calculated values of $\psi_c$ and the experimental cutoff angles provides a test of the proposed scattering potential.

We have measured the $\psi$ dependence to determine the cutoff angle for $Li^+$, $Na^+$, and $K^+$ scattered from a Mo(001) surface. This was done for incident-ion energies of 250, 500, and 2500 eV as a function of laboratory scattering angle $\theta$ between 20° and 110°. The results are compared with predicted values for TFM and ZBL scattering potentials. Although generally good agreement is obtained, there are also systematic discrepancies. These discrepancies are discussed with regard to the chain approximation and adequacy of a pairwise potential function.

## II. EXPERIMENTAL

The ion scattering spectrometer has been described previously.[5] The critical point in this experiment is the accurate measurement of the polar incident angle $\psi$. Accurate determination of the cutoff angles depends upon the calibration of the angle $\psi$, the repeatability of positioning the rotary feedthrough upon which the sample is mounted, the movements of the sample as a result of heating and cooling cycles, and the divergence of the beam line. The angle was calibrated by replacing the source with a viewport and directing a laser down the beam line under vacuum. The angle corresponding to $\psi=90°$, resulting in reflection of the laser straight back at the last aperture of the beam line, could be determined to within the readability of the rotary. Using the laser it was also possible to ascertain that the beam line was centered on the sample for all incidence angles, i.e., that the sample surface was positioned on the axis of rotation of the rotary. The sample was checked by this alignment procedure repeatedly throughout the course of these experiments. With the aid of the reflected laser light it was also determined that the sample moved very little ($\Delta\psi<0.1°$) during anneals to the highest temperatures used and returned to the original position upon cooling. The rotary could be read to better than 0.5° and repeatability and accuracy was good, as verified by the precision of the data. The normalized intensities were usually averages of three to four measurements in between which the rotary was moved and repositioned, and the standard deviations were consistently small, so that the position of the edge could usually be determined to within a few tenths of a degree. The beam line has a maximum divergence of ±0.5°. Measurements made on different days or widely separated in time occasionally resulted in noticeable shifts in the position of the edge over a range of up to 0.7°. These shifts were attributed to redirecting the beam within the divergence of the beam line due to charging in the beam line or to redistribution of the emission across the source. The shifts may also have been due, in part, to effects of different impurity coverages. Considering all these factors, we believe that the reported cutoff angles are accurate to about ±0.5°.

The width of the edges measured in the $\psi$ dependence are, in principle, affected by divergence of the incident beam, the acceptance angle of the electrostatic analyzer (ESA), and the effect on the ESA acceptance angle of beam-spot spreading at grazing angles of incidence. Analysis of these instrumental effects showed that the expected broadening is less than the actual measured widths, indicating that broadening due to thermal effects and deviations from the chain approximation are principally responsible for the observed widths.

The sample was a Mo(001) single crystal mounted in ultrahigh vacuum (UHV) on a two-axis manipulator. It was cleaned and prepared as described previously[5] by heating in $O_2$ to remove carbon, and sputtering to remove oxygen and sulfur. The surface-impurity concentrations were less than 0.10 monolayers (ML) total impurities as determined by Auger-electron spectroscopy. The crystal was clamped on 0.25-mm Mo wires and was heated from behind by electron bombardment. All measurements discussed below were for scattering in the [110] azimuth. The azimuthal angle $\phi$ could be determined rapidly and approximately by the low energy electron diffraction (LEED) pattern, and was determined to within 1° by the dependence on the ion scattering intensity upon $\phi$ at grazing incident angle. The total laboratory scattering angle $\theta$ is accurate to within 1°.

## III. RESULTS

### A. Experimental results

Proper interpretation of the $\psi$ dependence of the ion-scattering intensity requires cognizance of the changes which occur in the energy distribution $N(E)$. Sample scattered $K^+$ energy distributions are shown in Fig. 1 for the case of incident 250-eV $K^+$ ions scattered through a total laboratory scattering angle of 90°. Two maxima at

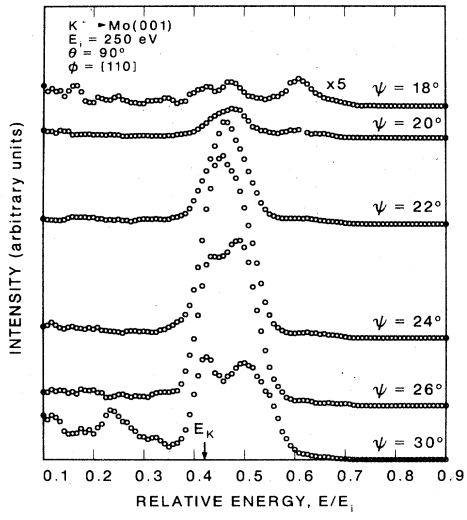


FIG. 1. Typical energy distributions of backscattered $K^+$ ions are shown as a function of $\psi$.

$E/E_i=0.425$ and 0.500 for the distribution obtained at $\psi=30°$ are due primarily to single and double scattering, respectively. The single scattering peak is quite close to the kinematical single scattering relative energy $E_k/E_i=0.421$. As $\psi$ is decreased, the two peaks shift together and the overall peak intensity increases, reaching a maximum at $\psi=24°$ with the peak position at $E/E_i=0.48$. There is a sharp dropoff in intensity as $\psi$ decreased further. This behavior is exactly as predicted for scattering from atomic chains, as has been observed and discussed previously.[6] At still lower values of $\psi$, single and multiple scattering features are again observed with much lower intensity and are attributed to scattering from steps and defects.

The details of how $N(E)$ evolves with $\psi$ depends in a complicated way upon the incident energy, total scattering angle, and the type of ion. The single and double scattering features for $K^+$ are more easily resolved at higher $E_i$ and larger $\theta$. At the lowest values of $\theta$ the features are not resolved at any value of $\psi$. A separate double-scattering peak at energies above the single-scattering peak was never observed in $Li^+$ scattering. Double scattering of $Na^+$ was observed but was not as well resolved as for $K^+$, a result predictable from the kinematics.

In every case, however, $N(E)$ is characterized by a single peak at the value of $\psi$ near where the intensity is largest, as illustrated in Fig. 1. This result is consistent with scattering from atomic chains since near the critical angle the single and double scattering are indistinguishable.[6] This suggests the procedure that was used to measure the cutoff angle. For given scattering conditions (i.e., $E_i$, $\theta$, and type of ion) the values of $\psi$ and $E$ which gave the maximum intensity, $\psi_{max}$ and $E_{max}$, were located. The ESA was then fixed at this energy and the count rate was measured as a function of $\psi$ over the range from just above $\psi_{max}$ down to angles sufficiently below it, so that the intensity dropped off to less than 20% of the maximum intensity. Occasionally the $\psi$ dependence was obtained by simultaneously varying the pass energy to stay on the single-scattering peak or by integrating the features in measured energy distributions. The position of the cutoff was generally independent of the method used.

A typical $\psi$ dependence is shown in Fig. 2. The same general shape was found for every ion and incident energy studied. The dependence is characterized by a fairly sharp cutoff in intensity at low $\psi$. The cutoff could be approximated by a straight line which fit the edge over the range from about 20—90 % of the maximum intensity. The linear fit was used to obtain a cutoff angle $\psi_{90}$ taken as the angle below $\psi_{max}$ where the intensity reaches 90% of the maximum. The origin of the assignment is discussed below. The values of $\psi_{90}$ are listed in Table I and shown in Fig. 3 for two exemplary cases. The widths of the edges, taken as the angle between 20% and 90% of maximum intensity, were found to vary from 2.1° to 3.8°. These widths are also given in Table I. The angular dependence exhibited a tail at low values of $\psi$ which was assumed to be due to scattering from surface defects. This tail was more intense when the peak in $N(E)$ was superimposed on a broad low energy background due to scattering from below the first layer, since such background was not subtracted in the technique used to determine the cutoff. This effect was very pronounced for 2500-eV $K^+$ ions at $\theta=110°$, where the peaks are at low relative energy and the background is sizable. It is believed that even for the worst case the accuracy of the cutoff determined is not seriously affected.

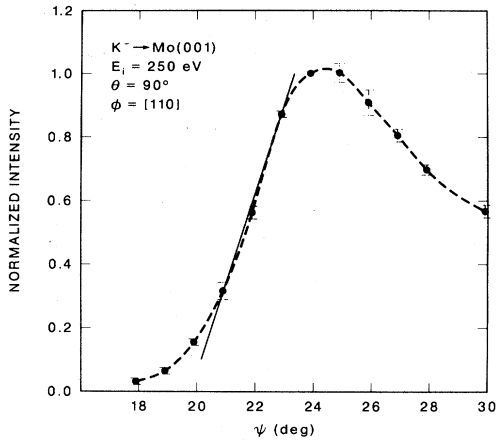


FIG. 2. Typical $\psi$ dependence is shown normalized to unit intensity at $\psi=24°$. The linear fit to the edge is used to obtain the width and $\psi_{90}$. The dashed curve guides the eye through the data. The error bars are $\pm 1\sigma$ on 3 to 4 measurements of the ratio of the intensity at a value of $\psi$ to that at $\psi=24°$.

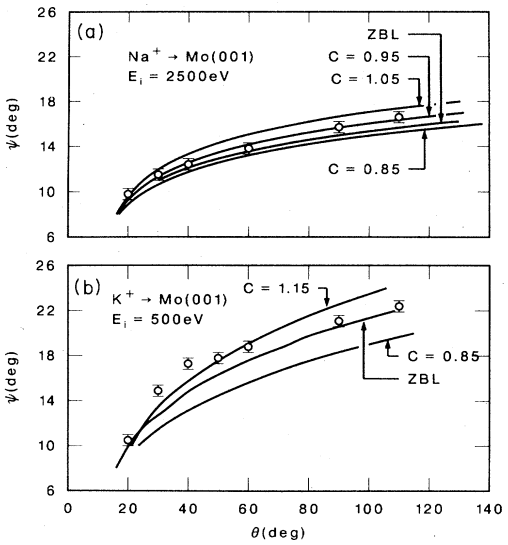


FIG. 3. Measured cutoff angles $\psi_{90}$ (points) are compared with the theoretical $\psi_c$ calculated for a ZBL potential [Eq. (3)] and for a TFM potential with various values of the screening length parameter $C$ [Eq. (2)]. These are shown for (a) 2500-eV $Na^+$ ions where, the agreement is good, and for (b) 500-eV $K^+$ ions where the experimental points deviate systematically from the calculated values. In (b) a curve calculated for the TFM potential with $C=1.0$ would be essentially indistinguishable from that shown for the ZBL potential.

TABLE I. Experimental cutoff angles, $\psi_{90}$, and edge widths (in parentheses). Angles and widths are in degrees.

| | $\theta$[a] | $E_i=250$[b] | $E_i=500$ | $E_i=2500$ |
|---|---|---|---|---|
| $Li^+$ | 20 | 10.3 (2.6) | 10.0 (2.8) | 9.3 (3.4) |
| | 30 | 13.1 (3.8) | 12.2 (2.7) | 10.7 (2.5) |
| | 40 | 13.8 (2.8) | 13.9 (2.9) | 11.5 (2.6) |
| | 60 | 15.8 (2.8) | 15.0 (2.4) | 12.2 (2.8) |
| | 90 | 17.4 (3.2) | 16.8 (3.1) | 13.2 (2.7) |
| | 110 | 18.5 (3.2) | 17.7 (3.1) | 13.7 (3.0) |
| $Na^+$ | 20 | 10.3 (2.3) | 10.4 (2.1) | 9.8 (2.1) |
| | 30 | 14.4 (3.0) | 14.0 (2.8) | 11.5 (2.2) |
| | 40 | 15.9 (2.8) | 15.3 (2.8) | 12.4 (2.1) |
| | 60 | 18.1 (2.8) | 17.4 (3.0) | 13.8 (3.0) |
| | 90 | 20.6 (2.8) | 19.4 (2.5) | 15.6 (2.9) |
| | 110 | 22.0 (3.0) | 20.8 (3.1) | 16.6 (3.3) |
| $K^+$ | 20 | | 10.5 (2.3) | 9.3 (2.2) |
| | 30 | 14.9 (2.7) | 14.9 (2.8) | |
| | 40 | 17.6 (3.5) | 17.3 (3.7) | 12.9 (2.5) |
| | 50 | | 17.8 (3.3) | |
| | 60 | 19.9 (2.8) | 18.8 (3.1) | 14.8 (2.8) |
| | 90 | 23.0 (2.5) | 21.1 (3.0) | 16.8 (3.3) |
| | 110 | 24.5 (3.0) | 22.4 (3.6) | 17.4 (3.2) |

[a]Laboratory scattering angles in degrees.
[b]Incident energy in eV.

It is important to consider the effects of impurities on the measured cutoff angles. The principal impurities were oxygen, carbon, and sulfur atoms deposited on the surface from CO, $CO_2$, $H_2S$, and $S_2$, which were present in the ambient. The effects of high coverages of oxygen and carbon on the $\psi$ dependence has been reported previously,[7] for 500-eV $Li^+$ ions scattered through 60°. The results showed that the sharp cutoff and peak at $\psi_{max}$ characteristic of the clean surface remain even for coverages up to 0.75 ML of oxygen or carbon. However, the intensity of the peak is decreased with respect to a broad maximum which grows at larger $\psi$ and dominates at high coverage. The peak is shifted less than 2° toward higher $\psi$ for a surface with 0.66 ML of oxygen compared to the clean surface. Similar results were reported for carbon and have been measured for sulfur layers with coverages of $\lesssim 0.5$ ML, and for both cases the shift relative to the clean surface is perhaps even less than for oxygen. It is therefore concluded that for coverages of $\lesssim 0.1$ ML of impurities the measured cutoff should be shifted less than 0.5° from the value for an ideally clean surface. This conclusion was also tested for 500-eV $K^+$ at $\theta=110°$ by oxygen adsorption and the same qualitative behavior was obtained.

### B. Computed results

#### 1. The critical angles

The computer simulations were performed using the code MARLOWE (version 12.0) described elsewhere.[8] Although the full three-dimensional structure of the Mo(001) surface (assumed to be unrelaxed with bulk termination) was used, only chainlike scattering was considered in calculating the critical angles. This was done by choosing trajectories in which the primary particles were incident in a single $(1\bar{1}0)$ plane containing a [110] chain of surface atoms with atoms separated by $\sqrt{2}a_0$ ($a_0=3.15$ Å, the Mo lattice constant). Since second-layer

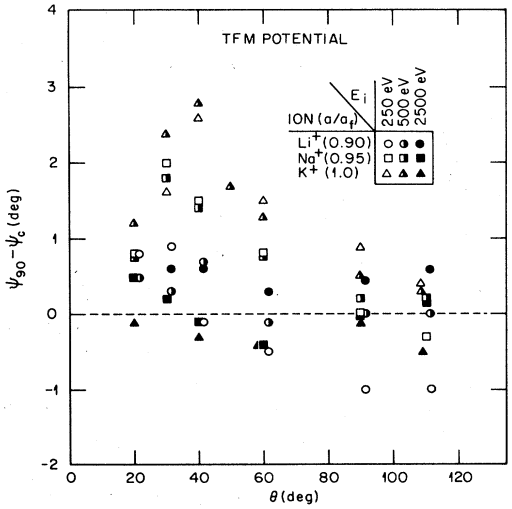


FIG. 4. Deviation between the measured and theoretical cutoff angles, $\psi_{90}-\psi_c$, is shown for three different ions at three different incident energies as a function of laboratory scattering angle. (For clarity some points are displaced slightly in $\theta$.) The values of $\psi_c$ are calculated using a TFM potential and the indicated values of $C=a/a_F$. The estimated error in $\psi_{90}-\psi_c$ is about ±0.5°.

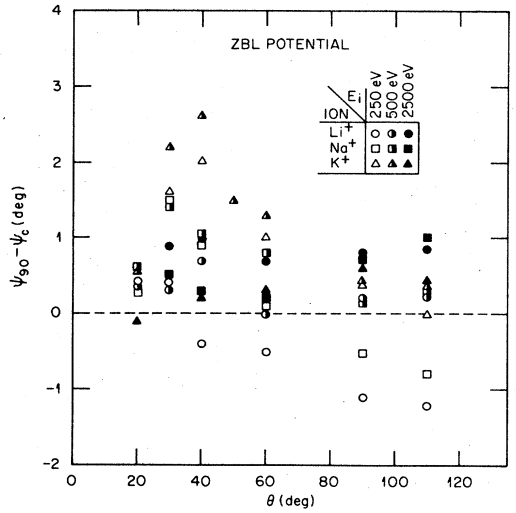


FIG. 5. Same as for Fig. 4, except the values of $\psi_c$ are calculated using a ZBL potential.

atoms are contained in this scattering plane at positions halfway between and $a_0/2$ below the first-layer atoms, they contribute slightly to the scattering. Neighboring chains of Mo atoms which lie at $a_0/\sqrt{2}$ away also contribute to the scattering, but their effect is very small. No thermal displacements of the ions from their ideal lattice sites were included.

The total scattering angle and final energy of the primaries were calculated as a function of the impact parameter along the chain. This was done for various values of $\psi$ for each ion and incident energy. Below a certain incident angle the chain becomes totally reflecting, so that no particles penetrate below the first layer. For each of the lower values of $\psi$, there is a corresponding minimum and maximum scattering angle, $\theta_{\min}$ and $\theta_{\max}$. Because of shadowing along the incident path, scattering cannot occur with scattering angles larger than $\theta_{\max}$, and because of blocking along the exit path, scattering cannot occur with scattering angles less than $\theta_{\min}$. The values $\theta_{\max}$ and $\theta_{\min}$ are easily obtained from inspection of the calculated $\theta$ as a function of impact parameter. A value of $\psi$ giving rise to a particular $\theta_{\max}$ is the critical value for that scattering angle. Calculating $\theta_{\max}$ as a function of $\psi$ is therefore identically equivalent to determining $\psi_c$ as a function of $\theta$.

The critical angles $\psi_c$ for each ion and incident energy were computed as a function of $\theta$ for the TFM and ZBL potentials. Sample results are shown in Fig. 3, where they are compared with the experimentally obtained values $\psi_{90}$. All of the data are shown in Figs. 4 and 5, where the difference between the computed $\psi_c$ and the experimental $\psi_{90}$ is shown as a function of laboratory scattering angle for each type of ion and each incident energy.

### 2. *Correspondence between $\psi_c$ and the measured $\psi$ dependence*

The critical angles $\psi_c$ calculated as described above are precisely defined. In any experiment, however, the $\psi$ dependence is broadened by thermal vibrations, surface defects, and instrumental angular resolution, and appear as in Fig. 2. The question arises as to which part of the $\psi$ distribution corresponds to $\psi_c$.

To answer this question, calculations were made on a chain with thermal displacements included. Circular "detectors" were used which were positioned at several scattering angles and had an angular acceptance of 2.5° half-angle. As before, all primary particles were incident in a single $(1\bar{1}0)$ plane containing the mean positions of the [110] surface chain atoms. The calculation was done for a nondivergent 500-eV K beam at various incident angles between 11.5° and 21.5° for a ZBL potential. The 8000 trajectories run at each $\psi$ were incident with random impact parameters along the chain. The uncorrelated, three-dimensional thermal displacements were determined according to the Debye model [Debye temperature of 240 K (Ref. 9) and lattice temperature of 400 K]. Each detector collected a full energy distribution of scattered particles for each value of $\psi$. The energy distributions were folded with an instrument function appropriate to the resolution of the ESA.

The $\psi$ dependence computed in this manner resembled the experimental dependences (Fig. 6), except that the computed intensities dropped off faster with $\psi$ at angles above $\psi_{\max}$. The cutoffs had about the same widths as measured experimentally, ranging from 2.0° to 4.1° for different scattering angles (measured from 20% to 90% of the maximum intensities, as before). The correspondence between the $\psi$ dependence and $\psi_c$ appeared to depend upon scattering angle. For $\theta=60°$, $\psi_c$ corresponded to the angle where the intensity is 60% of the maximum intensity (Fig. 6), while for lower scattering angles, $\psi_c$ corresponded to the angle at 90% of maximum intensity.

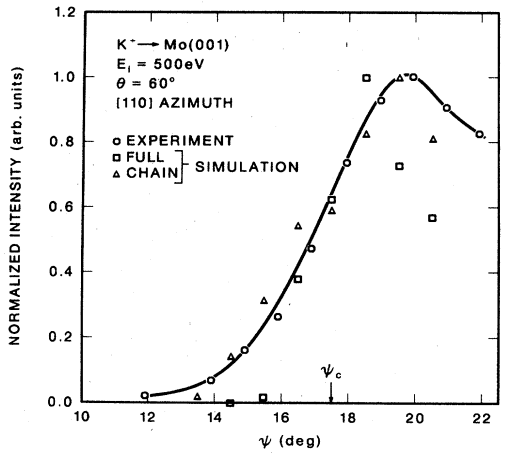


FIG. 6. Dependence of the ion-scattering intensity is shown as a function of the polar incident angle $\psi$ for experimental and computed data. The intensities are normalized to unit maximum intensity in each case. The dependence is computed both with and without the chain approximation using the ZBL potential. The errors are about 5%, 20%, and 25% for the experimental, chain, and full calculation, respectively. The curve guides the eye through the experimental data. The critical angle $\psi_c$ computed for a ZBL potential is also shown.

Since the statistical accuracy of the computed dependence was better at the low scattering angles, the 90% point $\psi_{90}$ was chosen for comparison with $\psi_c$. This assignment is a principal uncertainty in this method for determining the scattering potential.

### 3. *Validity of the chain model*

The [110] azimuth was chosen for all experiments because the scattering is nearly chainlike. Previous work has shown[5] that at other azimuths there are significant contributions from second-layer scattering and that focusing effects are present, especially near the [100] azimuth. Because of the geometry in the [110] azimuth, scattering from below the first layer does not contribute at energies near the single- and double-scattering peaks, and the scattering is chainlike except for some "zigzag" scattering. In this case, zigzag scattering means trajectories involving double scattering between two first-layer atoms which are not in the same [110] chain. Although zigzag scattering may be a major contribution under certain conditions, the important question is whether it can obscure, shift, or broaden the low-$\psi$ cutoffs measured with the present energy discrimination. It would appear from shadow-cone considerations that the effects of zigzag scattering would be greatest for large impact parameters and large shadow cones. These conditions correspond to small scattering angles and to low energies, especially for the more massive projectiles.

The validity of the chain model was tested by computer simulation. A calculation was done for 500-eV K under the same conditions as described in the preceding section, except that the restriction that the incident particles impact long the [110] chains was removed and instead incident impact points were distributed throughout the surface unit cell. Removing this restriction required that 20 000 trajectories be run at each incident angle to achieve statistical accuracy comparable to the chain calculation.

The resulting $\psi$ dependence for $\theta=60°$ is given in Fig. 6, where it is compared with the experimental $\psi$ dependence, and the $\psi$ dependence computed using the chain approximation. In this case, inclusion of the zigzag scattering has little effect on the position and width of the edge. At $\theta=40°$, the calculation using the full impact zone was shifted to larger $\psi$ by about 1.5°, so in this case the effect of the zigzag scattering is such that $\psi_{90}$ is an overestimate of $\psi_c$.

The conclusion from these calculations is that the chain approximation may indeed fail at the lower scattering angles, and it is expected that the effect will be largest at low incident energies. It is difficult to generalize the conditions under which the zigzag scattering will be the most significant, or to quantitatively predict how large the effect on $\psi_{90}$ would be for a given ion, $E_i$, or $\theta$.

## IV. DISCUSSION

The extent to which the experimentally measured cutoff angles $\psi_{90}$ agree with the calculated critical angles $\psi_c$ is shown in Figs. 4 and 5 for TFM and ZBL potentials, respectively. In the case of the TFM potential (Fig. 4) a different value of $C$ is chosen for each ion, these being 0.90, 0.95, and 1.0 for $Li^+$, $Na^+$, and $K^+$, respectively. These values were chosen to optimize agreement at the largest scattering angles for all three values of $E_i$. Reducing the value of $C$ has the effect of decreasing $\psi_c$, so that the points in Fig. 4 can be moved down or up by increasing or decreasing, respectively, the value of $C$. Using these values of $C$, it can be seen in Fig. 4 that the TFM potential predicts almost all cutoff angles to within $\pm 1°$ for $\theta \geq 60°$.

The best value of $C$ to use for describing ion scattering was discussed by O'Connor and McDonald.[10] They parametrized a large body of gas-phase scattering results to determine an effective screening function. They found that a reasonable agreement to a TFM potential was obtained if $C$ is chosen according to the formula

$$C = 0.69 + 0.0051(Z_1 + Z_2) . \tag{4}$$

The formula predicts $C$ values of 0.92, 0.96, and 1.0 for $Li^+$, $Na^+$, and $K^+$ on Mo, in excellent agreement with the results reported here.

Various researchers have compared the results of low-energy ion-scattering experiments with predictions based on the TFM potential. Heiland, Taglauer, and Robinson[11] compared measured $\theta_{min}$ and $\theta_{max}$ values for $Ne^+$ scattering from Ni, Ag, and W for $200 < E_i < 400$ eV. A sharp cutoff in intensity at $\theta_{max}$ was not observed, however, unless they considered the intensity ratios at two different azimuths. Using this method they deduced values of $C$ of 0.84, 1.04, and 1.04 for Ne on Ni, Ag, and W, respectively, which agree fairly well with the values predicted by Eq. (4) (0.88, 0.98, and 1.12 for Ne on Ni, Ag, and W, respectively). Poelsma, Verheij, and Boers[12] used three different techniques to determine the best values of $C$ for 10-keV inert-gas ions on Cu(100). They compared the measured cutoff in a $\psi$ dependence, the single scattering peak width, and double to single scattering peak intensity ratios with predictions obtained from computer simulations made within the chain-scattering approximation. Comparing the prediction of TFM potential with these results they obtained $C$ values of 0.69, 0.75, 0.73, and 0.91 for $He^+$, $Ne^+$, $Ar^+$, and $Kr^+$, respectively. These value are all low compared to the values predicted by Eq. (4) of 0.85, 0.89, 0.93, and 1.02 for $He^+$, $Ne^+$, $Ar^+$, and $Kr^+$, respectively. As discussed by the authors, the effects of neutralization and inelastic losses could make the experimental values too low. Aono *et al.*[13] studied $He^+$ on Ti and found that a TFM potential with $C=0.96$ to 1.0 [compared to 0.81 predicted by Eq. (4)] gave reasonable prediction of the measured cutoff angles for $E_i$ in the range of 500–2000 eV. They noted that there were systematic deviations which seemed to depend on impact parameter and incident energy. In studies of $K^+$ scattering from Au(110),[14] qualitative comparison of $E$-$\theta$ loops with the results of computer simulation indicated that a value of $C=1.0$ was appropriate for this system [compared to 1.19 predicted by Eq. (4)]. A more recent analysis which compared computed and experimental intensities confirmed the value of $C=1.0$.[15]

It can be seen in Fig. 5 that the ZBL potential gives results similar to those for the TFM potential. It is signifi-

cant that this potential gives an equal or even slightly better fit to all the data, even though there are no "adjustable" parameters. It was also found that upon comparison of the computed and experimental energy distributions the ZBL potential gave better agreement with experiment than the TFM potential. As described in a previous study,[16] varying the value of $C$ could not bring about a good fit to experiment for both the [100] and [110] azimuths. Use of a ZBL potential gave quite good agreement between experimental and computed energy distributions, as shown in Fig. 7. Simulations using essentially identical model parameters except for a TFM potential with $C=1.0$ gave substantially poorer overall agreement with respect to peak positions and intensity ratios.

Inspection of Fig. 3(b) reveals that there are systematic deviations from the predicted cutoff angle for both the TFM and ZBL potentials. The most noticeable trend is that at low scattering angles the experimental cutoff angle is larger than predicted by the models, especially for $K^+$. This is also apparent in Figs. 4 and 5. This effect depends upon incident energy, with the greatest deviations occurring at low energy, as seen in Fig. 4. For an incident energy of 2500 eV, the quantity $\psi_{90}-\psi_c$ is very nearly constant for all three ions varying over a range of only 0.3°, 0.9°, and 0.4° for $Li^+$, $Na^+$, and $K^+$, respectively. For 250 eV, however, the range of deviation is 1.9°, 2.3°, and 2.2° for $Li^+$, $Na^+$, and $K^+$, respectively. Thus, although the form of the TFM or ZBL potential fits the data quite well at 2500 eV, the fit is substantially poorer at 500 eV and below. It is also seen in Figs. 4 and 5 that the difference $\psi_{90}-\psi_c$ varies with $E_i$ and ion type more than expected from the experimental precision. No single value of $C$ can bring agreement at all three energies for a given ion. This is an indication that the form of the potential in Eq. (1) is not fully adequate.

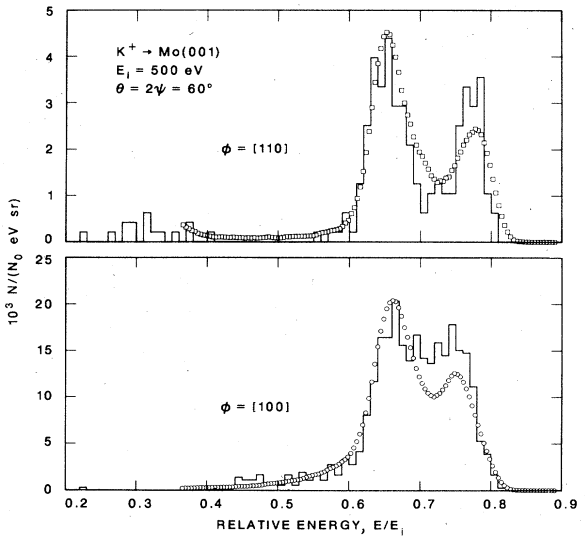


FIG. 7. Computed (histograms) and experimental (points) energy distributions are compared for scattering in two different azimuths of clean Mo(001). The intensity values refer to the computed distributions, while the experimental distributions are scaled so that the maximum intensity in the [100] azimuth is $20.4\times10^{-3}$ $eV^{-1}sr^{-1}$. The simulation was done using the ZBL potential and included the effects of thermal displacements, small inelastic losses, and a 1.0° divergence in the incident beam, and used an acceptance solid angle of 23.9 msr. The experimental distributions were corrected for the $1/E$ distortion of the ESA and used an acceptance solid angle of about 4.5 msr.

There are two possible causes for these systematic discrepancies: First, the possible inappropriateness of the scattering potential and, second, a breakdown of the chain approximation. The deviations at low scattering angle are most evident at 250 eV for every ion, but are absent within experimental error at 2500 eV. This suggests that at low energies a pairwise scattering potential is not sufficient. The sign of the deviation, i.e., larger values of $\psi_{90}-\psi_c$ at low scattering angles, is consistent with a more repulsive potential at larger impact parameters than provided by the pairwise potential. This is exactly the result expected if there is an additional $z$-dependent repulsive potential such as that proposed by Hulpke and Mann.[4] In this regard it is interesting to note the differences between the TFM and ZBL potentials. For K on Mo the ZBL potential decreases with $r$ slightly faster than does the TFM potential (with $C=1.0$) out to about 1.0 Å. However, the ZBL potential falls off more slowly for $r>1.0$ Å than does the TFM, so that at separations of about $a_0/\sqrt{2}\sim2.2$ Å (i.e., halfway between chain atoms) the ZBL potential is 50% larger than TFM potential. The ZBL potential then provides a greater repulsive potential in the regions centered between surface atoms, as called for by the results of Mann and Hulpke.[4] This might contribute to the improvement in the computer-simulated energy distributions obtained using the ZBL potential.

A second possible cause of the deviations at low scattering angle is a breakdown in the chain model or the technique. As described above, the effect of extensive zigzag scattering is expected to make the values of $\psi_{90}$ too large, and the effect is expected to be worse at low incident and scattering angles. These facts are consistent with the observed increase of $\psi_{90}-\psi_c$ at low angles. Also, the technique of assigning a point of fixed relative intensity to the critical angle may also introduce errors since the correspondence between $\psi_c$ and the thermally broadened cutoff may depend upon scattering angle. This could also lead to systematic deviation in $\psi_{90}-\psi_c$ with $\theta$.

On the basis of the work presented, we cannot decide between these two possibilities. It is, in principle, possible to analyze the breakdown of the chain model by computer simulation. It is also possible to avoid the chain approximation altogether by comparing the measured and simulated $\psi$ dependences directly, adjusting the scattering potential to give a best fit. However, the computer time required for either approach would be formidable. To our knowledge no analytical means of approaching this problem is available. The effect of a potential function with a $z$ dependence could be included in a computer simulation, but this capability is not currently available in MARLOWE.

## V. SUMMARY AND CONCLUSIONS

The cutoff angle has been measured in the [110] azimuth on a clean Mo(001) surface. This was done using

$Li^+$, $Na^+$, and $K^+$ ions of incident energies 250, 500, and 2500 eV and total scattering angles between 20° and 110°. The measured angles were compared with angles predicted by the chain model for two different scattering potentials. The fundamental conclusions are as follows: (i) The cutoff angles are predicted to within 1° by either the TFM or the ZBL potentials for incident energies of 2500 eV. (ii) Use of the TFM potential requires adjustment of the screening length to a value different than the Firsov value by a factor which is adequately given by the empirical formula O'Connor and McDonald. (iii) The ZBL form of the screening length works well with the ZBL potential for all three ions. (iv) At low energies ($E_i \lesssim 250$ eV) and small scattering angles ($\theta \lesssim 60°$) the cutoff angles are larger than predicted by either the TFM or the ZBL potentials. This deviation is consistent with an underestimate of the actual repulsive potential at large separations, but the possibility exists that the deviation is due to breakdown of the chain approximation.

## ACKNOWLEDGMENTS

Research was sponsored by the Division of Chemical Sciences (Office of Basic Energy Sciences), U.S. Department of Energy, under Contract No. DE-AC05-840R21400 with the Martin Marietta Energy Systems, Inc. The authors wish to thank O. S. Oen and J. H. Barrett for critically reading the manuscript.

[1]G. Moliere, Z. Naturforsch. Teil A **2**, 133 (1947).
[2]O. Firsov, Zh. Eksp. Teor. Fiz. **33**, 696 (1958) [Sov. Phys.—JETP **6**, 534 (1958)].
[3]J. F. Ziegler, J. P. Biersack, and U. Littmark, Oak Ridge National Laboratory, Report No. CONF-820131 (unpublished).
[4]E. Hulpke and K. Mann, Surf. Sci. **133**, 171 (1983).
[5]S. H. Overbury, P. C. Stair, and P. A. Agron, Surf. Sci. **125**, 377 (1983).
[6]A. Boers, Surf. Sci. **63**, 475 (1977).
[7]S. H. Overbury and P. C. Stair, J. Vac. Sci. Technol. A **1**, 1055 (1983).
[8]M. T. Robinson, *Sputtering by Particle Bombardment I,* Vol. 47 of *Topics in Applied Physics,* edited by R. Behrisch (Springer, Heidelberg, 1981), p. 73.
[9]D. P. Jackson, Surf. Sci. **43**, 431 (1974).
[10]D. J. O'Connor and R. J. MacDonald, Radiat. Eff. **34**, 247 (1977).
[11]W. Heiland, E. Taglauer, and M. T. Robinson, Nucl. Instrum. Methods **132**, 655 (1976).
[12]B. Poelsema, L. K. Verhey, and A. L. Boers, Surf. Sci. **64**, 554 (1977).
[13]M. Aono, Y. Hou, R. Souda, C. Oshima, S. Otani, Y. Ishizawa, K. Matsuda, and R. Shimizu, Jpn. J. Appl. Phys. **21**, L670 (1982).
[14]S. H. Overbury, W. Heiland, D. M. Zehner, S. Datz, and R. S. Thoe, Surf. Sci. **109**, 239 (1981).
[15]H. Hemme and W. Heiland, Nucl. Instrum. Methods B **9**, 41 (1985).
[16]S. H. Overbury, Nucl. Instrum. Methods B **2**, 448 (1984).